

Supplemental Data

Generation of Robust Left-Right Asymmetry in the Mouse Embryo Requires a

Self-Enhancement and Lateral-Inhibition System

Tetsuya Nakamura, Naoki Mine, Etsushi Nakaguchi, Atsushi Mochizuki,
Masamichi Yamamoto, Kenta Yashiro, Chikara Meno, and Hiroshi Hamada

Mathematical model formulation

We built a mathematical model based on the self-enhancement and lateral-inhibition system, and the principle proposed by Turing (1952) and Meinhardt and Gierer (2000). The formulas of the mathematical model can be written as follows in general.

$$\begin{aligned}\frac{\partial N}{\partial t} &= D_N \Delta N + f(Z) - d_N N \\ \frac{\partial L}{\partial t} &= D_L \Delta L + g(Z) - d_L L \\ \frac{\partial P}{\partial t} &= I(Z) - d_p P + H(P)\end{aligned}\tag{1}$$

where N , L and P are the levels of Nodal, Lefty and Pitx2, respectively. $Z = aN - bL$ is the level of the net induction signal. $f(Z)$, $g(Z)$ and $I(Z)$ are the synthesis rates of Nodal, Lefty and Pitx2, respectively. They are increasing functions of Z , thus increasing functions of N , and decreasing functions of L . $H(P)$ is the synthesis rate of Pitx2 during the period when Pitx2 expression is maintained. This is also an increasing function of P .

We assumed that the rates of transcription and degradation of mRNA are large enough and the dynamics of mRNA are always at the equilibrium. We also assumed that the protein synthesis rates are so called switching function of Z , i.e. $f(Z)$, $g(Z)$ and $I(Z)$ are close to 0 when Z is small, increase rapidly when Z is near the threshold value, and saturate at plateau values when Z is large. The plateau value of $f(Z)$, $g(Z)$ or $I(Z)$ should be large enough relative to the degradation rate d . The thresholds of $f(Z)$, $g(Z)$ and $I(Z)$ are $Z = T_N$, $Z = T_L$ and $Z = T_p$ respectively. T_N and T_L are close, but experimental

data suggest that T_N is smaller than T_L . The function $H(P)$ is also assumed to have the similar properties as above.

Our model is similar to the one called activator-inhibitor system proposed by Gierer and Meinhardt (1972). The model shows spatially periodic patterns based on the principle of diffusion-induced instability formalized by Turing (1952). However, we do not focus on the diffusion-induced instability here because the purpose of our modeling is not to study the mechanism for generating spatial periodicity.

Qualitative Behavior of Nodal and Lefty

Qualitative behavior of this model can be simply understood as shown below. First we studied the behavior of the reaction term of the model (1) excluding the diffusion terms and nodal flow. The dynamics of the ordinary differential equations of two variables N and L

$$\begin{aligned}\frac{dN}{dt} &= f(Z) - d_N N \\ \frac{dL}{dt} &= g(Z) - d_L L\end{aligned}\tag{2}$$

can be understood easily by simple analysis, e.g. isocline analysis. From the assumption of switching forms of $f(Z)$ and $g(Z)$, $f(Z)$ and $g(Z)$ can be approximated to linear functions of slope α and β near the thresholds $Z = T_N$ and $Z = T_L$, where $\alpha = f'(T_N)$ and $\beta = g'(T_L)$, respectively and this approximation does not affect the nature of dynamics. Therefore, the isocline can be approximated into two lines within a finite area of N and L ($0 < N < N_{\max}$, $0 < L < L_{\max}$). The line for N is $\alpha(aN - bL - T_N) - d_N N = 0$, and that for L is $\beta(aN - bL - T_L) - d_L L = 0$. Let (N^*, L^*) denote intersection point of two isoclines. There are two typical cases in which two isoclines intersect within the area (Case I and Case II) and one case in which two isoclines do not intersect (Case III) within the area.

Case I: Signal-dependent amplification ($\frac{\beta b + d_L}{\beta b} < \frac{\alpha a}{\alpha a - d_N} < \frac{T_L}{T_N}$)

In this case, there are three equilibriums. The equilibrium at the intersection point (N^*, L^*) may be a stable or unstable equilibrium depending on the parameter values. The second equilibrium, origin of the space, is always stable. The last equilibrium is located on the N -axis and is always unstable. There are two distinct dynamical trajectories depending on the initial condition as seen in Figure 2B. We consider that the initial condition is located on the N -axis in Figure 2B, which represents the actual

situation of LPM that receives Nodal signal. The initial level of N (N_i) depends on a time integral of $E(t, x)$. If N_i is small enough, N and L would decrease and converge to the origin (dynamics \aleph in Figure 3B). If N_i is large enough, the level of N will increase by inducing self-activation. If the intersection point (N^*, L^*) is stable, the dynamics will converge to the intersection point (Figure S2A). However, if the intersection point (N^*, L^*) is unstable, the dynamics of (N, L) will converge to the origin after the temporal amplification (Figure 3B), which is what we indeed observe in the left LPM of the mouse embryo. The condition for the point (N^*, L^*) to be unstable is $\alpha a - \beta b > d_N + d_L$. When the point (N^*, L^*) is unstable, the behavior of signal-dependent amplification of N and L is as follows.

- (1) (N, L) directly converges to zero when N_i is small (red arrow, Figure 3B), or
- (2) (N, L) shows temporal amplification when N_i is large (blue line, Figure 3B),

The inequality $\alpha a > \beta b + d_N + d_L$ and the first inequality of the Case I conditions $\alpha a / d_N < \beta b / d_L + 1$ are the requirements for the pattern shown in Figure 3B to appear. Thus, this pattern appears only when self-induction rate of Nodal (αa) is larger than the sum of self-repression of Lefty and degradation rates ($\beta b + d_N + d_L$). Furthermore, a self-induction rate relative to a degradation rate of Nodal ($\alpha a / d_N$) must be much smaller than a relative repression rate of Lefty ($\beta b / d_L$). The degradation rate of Nodal (d_N) must be sufficiently larger than that of Lefty (d_L) to satisfy the latter condition above.

Case II: Bi-stable ($\frac{\alpha a}{\alpha a - d_N} < \frac{\beta b + d_L}{\beta b}$)

In this case, there are three equilibriums. The equilibrium at the intersection point (N^*, L^*) is always unstable. Two remaining equilibriums, one at the origin and the other at the maximum N , are always stable. Therefore, this system is bi-stable. The dynamics of the system in this case converges either to the maximum or minimum depending on the initial condition. Two different patterns of dynamics are shown in Figure S2B, C.

Case III: Stable at the origin ($\frac{T_L}{T_N}, \frac{\beta b + d_L}{\beta b} < \frac{\alpha a}{\alpha a - d_N}$)

In this case, there is only one equilibrium at the origin, which is stable. The dynamics of the system in this case converges to the origin. This dynamics also mimics *Nodal* and *Lefty* expression patterns observed in the mouse embryo. However, this case is unlikely to take place in the mouse embryo, because $0 < T_N < T_L$ (suggested by previous

experimental data) and $0 \ll \alpha, \beta$.

Diffusion Effects on Qualitative Behavior

After analyzing qualitative behavior of formula (1) without diffusion terms, diffusion effects were integrated into the unstable pattern of Case I, which most likely explain Nodal and Lefty expression patterns in the embryo. When diffusion terms are added to the lines of N and L given by formula (2), lines for N and L become $D_N \Delta N + \alpha(aN - bL - T_N) - d_N N = 0$ and $D_L \Delta L + \beta(aN - bL - T_L) - d_L L = 0$, respectively.

In the right LPM, diffusion effects shift the lines of N and L upward (FigS2E: upward because the levels of Nodal and Lefty that diffuse away from right LPM are smaller than the levels of Nodal and Lefty that reach right LPM; green arrows). The dotted lines are “space-free” lines. The shift of the line for L is larger than that for N because the diffusion coefficient for Lefty is larger than that for Nodal. Then equilibrium that is identical to “0” in case of “space-free” also shifts upward, which is denoted as “0*”. In left LPM, however, diffusion effects do not change the pattern of isocline, because a greater number of Nodal and Lefty diffuse away from left LPM than they reach left LPM, which shifts the lines of N and L downward (Fig.S2F: green arrows). Then equilibrium that is identical to “0” in case of “space-free” also shifts downward, which is denoted as “0*”. Thus, diffusion effects drastically change the dynamics of N and L only in right LPM. These changes of dynamics in left and right LPM can explain our experimental data obtained by RT-PCR (Figure 7)

Qualitative Behavior of Pitx2

We consider qualitative behavior of Pitx2 by the terms, “ $H(P)$ ” and “ $d_P \times P$ ”, because the term “ $I(Z)$ ” shown in formula (1) is an induction term of Pitx2 by Nodal signal and this term becomes “0” after temporal up-regulation of Nodal and Lefty. We then consider the following differential equation.

$$\frac{dP}{dt} = H(P) - d_P \times P = M(P)$$

If $H(P)$ is a switching function like $f(Z)$, $g(Z)$ or $I(Z)$, then $M(P)$ is a bi-stable function and the bi-stable points are $P_0 (= 0)$ and $P_s (P_s > 0)$. If induction of Pitx2 by Nodal signal is sufficiently large ($P > T_l$: the value of T_l is close to that of T_q , which is a threshold

value of Pitx2 persistence), the level of Pitx2 converges to P_s . However, when induction of Pitx2 is small ($P < T_l$), the level of Pitx2 converges to P_0 .

A Computer Simulation of the Mathematical Model

We performed computer simulations with the use of MATHEMATICA software as following.

< Nodal >

$$\frac{\partial N}{\partial t} = D_N \times \Delta N + \frac{s_N}{1 + \text{Exp}[-\lambda_N \times (g_N \times N - g_L \times L - T_N)]} - d_N \times N + E(t, x)$$

< Lefty >

$$\frac{\partial L}{\partial t} = D_L \times \Delta L + \frac{s_L}{1 + \text{Exp}[-\lambda_L \times (g_N \times N - g_L \times L - T_L)]} - d_L \times L$$

< Pitx2 >

$$\frac{\partial P}{\partial t} = \frac{s_p}{1 + \text{Exp}[-\lambda_p \times (g_N \times N - g_L \times L - T_p)]} - d_p \times P + \frac{s_q}{1 + \text{Exp}[-\lambda_q \times (P - T_q)]}$$

$$\begin{aligned}
& \langle \text{Nodal Flow} \rangle \\
E(t,x) &= \begin{cases} f_{i1} \times U(t - m_1) & (\text{in right LPM}) \\ f_{i0} \times U(t - m_0) & (\text{in midline}) \\ f_{i2} \times U(t - m_2) & (\text{in left LPM}) \\ 0 & (\text{else}) \end{cases} \\
\\
U(t) &= \begin{cases} 0 & (\text{if } t < 0.75) \\ 2t - 1.5 & (\text{if } 0.75 \leq t < 12.875) \\ -2t + 50 & (\text{if } 12.875 \leq t < 25) \\ 0 & (\text{if } 25 \leq t) \end{cases}
\end{aligned}$$

The model includes three partial differential equations for three components Nodal N , Lefty L , and Pitx2 P .

Positioning of Embryonic Regions

For simulation, the embryo is divided into seven domains: right yolk sac, right LPM, right PAM, the midline, left PAM, left LPM and left yolk sac (Figure 3F). Parameters for the midline, left LPM, and right LPM are denoted with a subscript of 0, 1, and 2, respectively (for example, T_{N0} , T_{N1} , and T_{N2}). In the PAM and yolk sac that lack Cryptic, an essential component of Nodal signaling, the synthesis rates are set at 0.

Nodal Flow

Nodal flow, the leftward flow of the extra-embryonic fluid in the node is essential for breaking symmetry. The nodal flow term, $E(t,x)$, was added to the differential equation of Nodal, because *Nodal* expression produced in the node is required for *Nodal* expression in LPM (Brennan et al.,2002; Saijoh et al.,2003). m for LPM is larger than that for midline, because it would take slightly longer time for the activating signal to reach LPM than to

reach the node. f_i is the level of the initial activation signal regulated by nodal flow. Because nodal flow travels from the right to the left in the node, f_i for Left LPM (f_{i1}) is larger than that for right LPM (f_{i2}) in the wild-type embryo.

Persistent Expression of *Pitx2*

Asymmetric *Pitx2* expression begins similarly in left LPM, but persists for a long period (additional few days), unlike *Nodal* and *Lefty2*. Thus, *Pitx2* expression is regulated by two-steps: induced by Nodal-FoxH1 pathway, and then maintained by Nkx2 (Shiratori et al., 2001). However, it is unknown how the activity of Nkx2 is regulated in this process. Therefore, we set *Pitx2* differentiation equation as following. First, *Pitx2* expression (P) is initiated by the similar formulation as *Nodal* and *Lefty*. Second, once the level of *Pitx2* exceeds a threshold value (T_q), *Pitx2* expression persists (by *Pitx2* expression rate: b_q).

Parameter Condition

T is the minimum level of induction signal required to initiate synthesis. s is rate of synthesis. The equations have an upper limit of synthesis rate. g_N is an efficiency constant of Nodal-mediated activation. g_L is an efficiency constant of *Lefty*-mediated inhibition. T_N is set lower than T_L in LPM because the asymmetric enhancer (ASE) of *Nodal* is more sensitive to the Nodal signal than is that of *Lefty1* or *Lefty2* (C.M. et al., unpublished data) and because *Nodal* expression begins in left LPM earlier than does *Lefty2* expression. At the midline, $T_L < T_N = T_P$, because *Lefty1* mRNA expression begins earliest and achieves the highest level. d are degradation rates and d_L is smaller than d_N , that is *Lefty* is probably more stable than is *Nodal* because the expression of *Lefty2* mRNA persists longer than *Nodal* mRNA in LPM. The diffusion coefficient D_N is smaller than D_L , because *Lefty1* and *Lefty2* may diffuse faster than does *Nodal*.

Parameter Setting

The exact values of the parameters used for each type of mouse are summarized in Supplementary Table S1. With these parameter sets, we could simulate the expression patterns of *Nodal*, *Lefty1*, *Lefty2*, and *Pitx2* in wild-type and various mutant mice. However, there are possibilities of other combinations of parameter sets that can also simulate gene expression patterns. Furthermore it should be noted that all parameters are dimensionless and our results of simulations have no information on scale and units.

Expression patterns in the wild-type mouse are as follows.

- 1) *Lefty1* mRNA appears at Midline before *Nodal* and *Lefty2* mRNA appear at LPM
- 2) *Nodal* mRNA appears in left LPM slightly earlier than *Lefty2* mRNA does so.
- 3) *Nodal* mRNA and *Lefty2* mRNA are present in left LPM in a transient manner.
- 4) *Nodal* mRNA disappears from left LPM earlier than *Lefty2* mRNA does so.
- 5) *Pitx2* mRNA appears in left LPM and persists.

The feature constraints for *Lefty1* mutant are i) *Nodal* mRNA appears only in Left LPM and ii) the *Lefty2* mRNA level at Midline is higher than that of the wild-type embryo. In *Lefty1* mutant simulation, we reduced S_{L0} to 10% of the wild-type value, because of a redundancy with *Lefty2*. The constraints for the *Lefty2* mutant are i) *Nodal* mRNA expression appears only in left LPM and ii) the *Lefty1* mRNA level at Midline is higher than that for the wild-type embryo. In the *Lefty2* mutant simulation, *Nodal* expression in left LPM persists and does not disappear. In the mutant embryo *in vivo*, however, *Nodal* expression subsequently disappears because expression of *FAST* and *Cryptic* is lost at the 6-7somite stage. The level of mRNA needs to exceed a certain level to be experimentally detected by *in situ* hybridization: for example, expression at a low level such as shown in the right LPM of *iv/iv* (L) embryo (Fig. S3E) would be undetectable by *in situ* hybridization.

Supplemental References

- Brennan, J., Norris, D.P., and Robertson, E.J. (2002). Nodal activity in the node governs left-right asymmetry. *Genes Dev.* *16*, 2339–2344.
- Collignon, J., Varlet, I., and Robertson, E.J. (1996). Relationship between asymmetric nodal expression and the direction of embryonic turning. *Nature* *381*, 155–158.
- Huangfu, D., Liu, A., Rakeman, A.S., Murcia, N.S., Niswander, L., and Anderson, K.V. (2003). Hedgehog signalling in the mouse requires intraflagellar transport proteins. *Nature* *426*, 83–87.
- Lowe, L.A., Supp, D.M., Sampath, K., Yokoyama, T., Wright, C.V., Potter, S.S., Overbeek, P., and Kuehn, M.R. (1996). Conserved left-right asymmetry of nodal expression and alterations in murine situs inversus. *Nature* *381*, 158–161.
- Marques, S., Borges, A.C., Silva, A.C., Freitas, S., Cordenonsi, M., and Belo, J.A. (2004).

- The activity of the Nodal antagonist Cerl-2 in the mouse node is required for correct L/R body axis. *Genes Dev.* *18*, 2342–2347.
- Meinhardt, H., and Gierer, A. (2000). Pattern formation by local self-activation and lateral inhibition. *Bioessays* *22*, 753–760.
- Meno, C., Shimono, A., Saijoh, Y., Yashiro, K., Mochida, K., Ohishi, S., Noji, S., Kondoh, H., and Hamada, H. (1998). *lefty-1* is required for left-right determination as a regulator of *lefty-2* and *nodal*. *Cell* *94*, 287–297.
- Meno, C., Takeuchi, J., Sakuma, R., Koshiba-Takeuchi, K., Ohishi, S., Saijoh, Y., Miyazaki, J., ten Dijke, P., Ogura, T., and Hamada, H. (2001). Diffusion of nodal signaling activity in the absence of the feedback inhibitor *Lefty2*. *Dev. Cell* *1*, 127–138.
- Murcia, N.S., Richards, W.G., Yoder, B.K., Mucenski, M.L., Dunlap, J.R., and Woychik, R.P. (2000). The Oak Ridge Polycystic Kidney (*orpk*) disease gene is required for left-right axis determination. *Development* *127*, 2347–2355.
- Saijoh, Y., Oki, S., Ohishi, S., and Hamada, H. (2003). Left-right patterning of the mouse lateral plate requires nodal produced in the node. *Dev. Biol.* *256*, 160–172.
- Shiratori, H., Sakuma, R., Watanabe, M., Hashiguchi, H., Mochida, K., Sakai, Y., Nishino, J., Saijoh, Y., Whitman, M., and Hamada, H. (2001). Two-step regulation of left-right asymmetric expression of *Pitx2*: initiation by nodal signaling and maintenance by *Nkx2*. *Mol. Cell* *7*, 137–149.
- Takeda, S., Yonekawa, Y., Tanaka, Y., Okada, Y., Nonaka, S., and Hirokawa, N. (1999). Left-right asymmetry and kinesin superfamily protein KIF3A: new insights in determination of laterality and mesoderm induction by *kif3A*^{-/-} mice analysis. *J. Cell Biol.* *145*, 825–836.
- Turing, A.M. (1952). The chemical basis of morphogenesis. *Phil. Trans. R.Soc.London* B237, 37-72

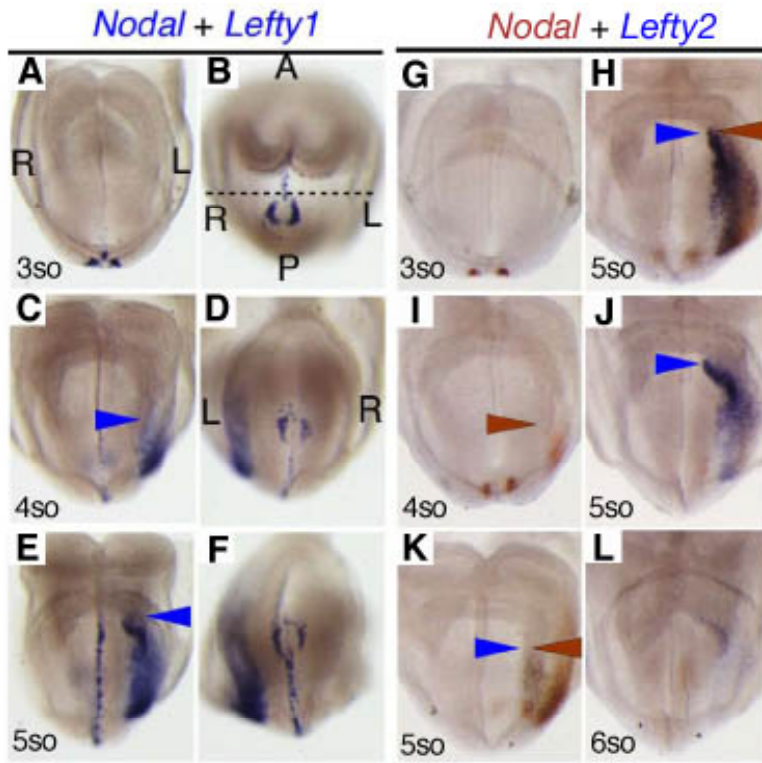


Figure S1

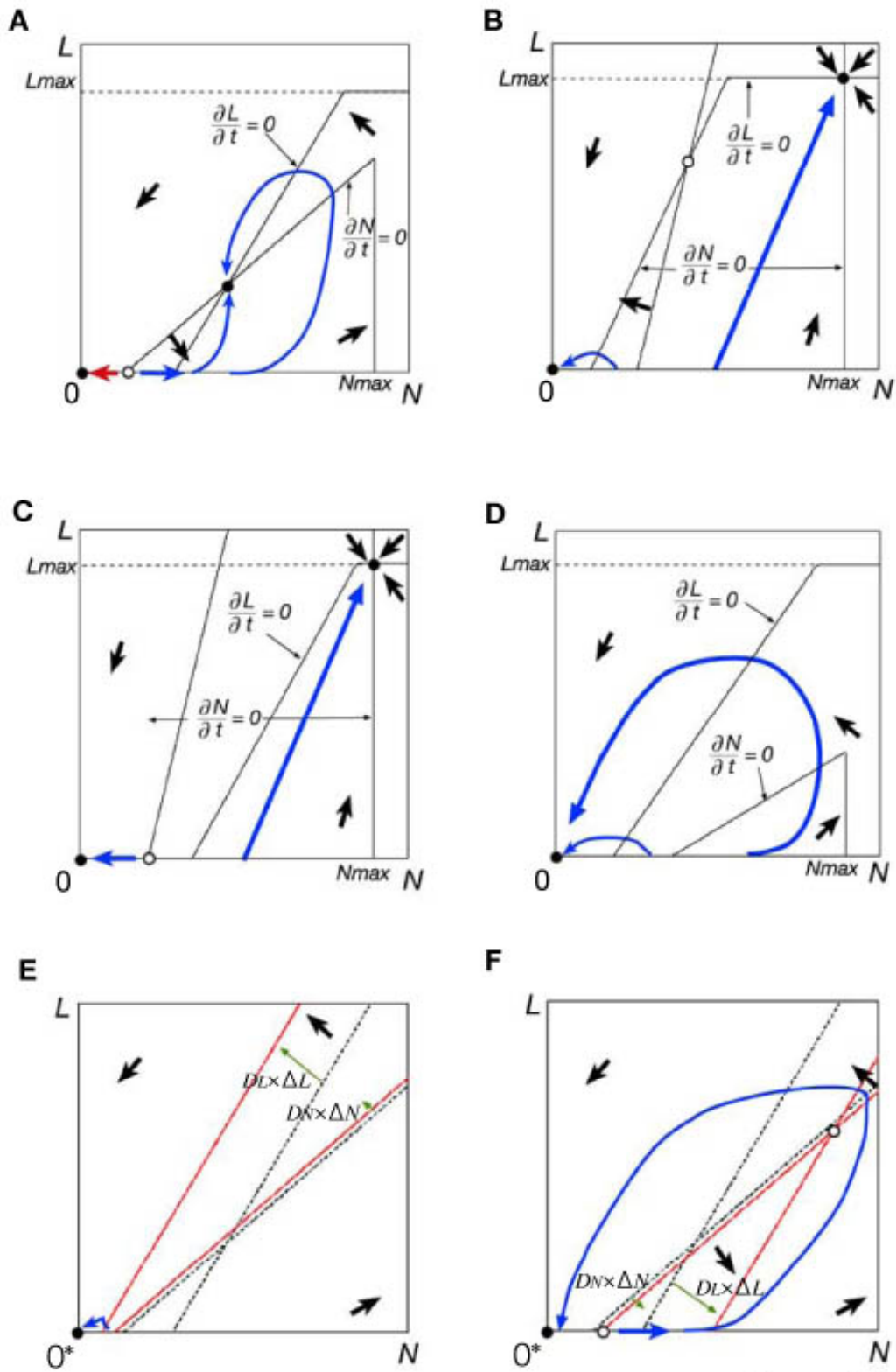


Figure S2

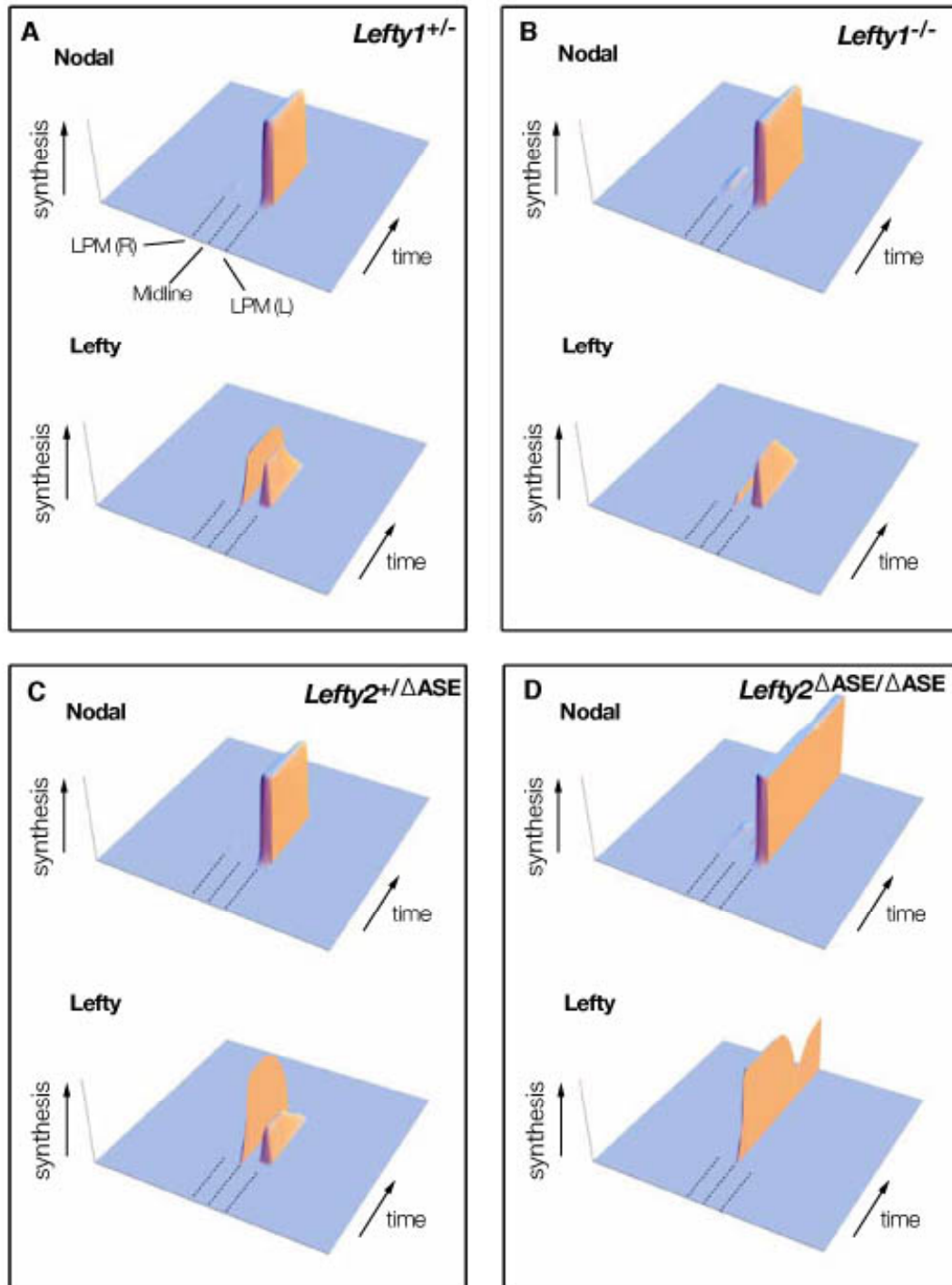


Figure S3-1

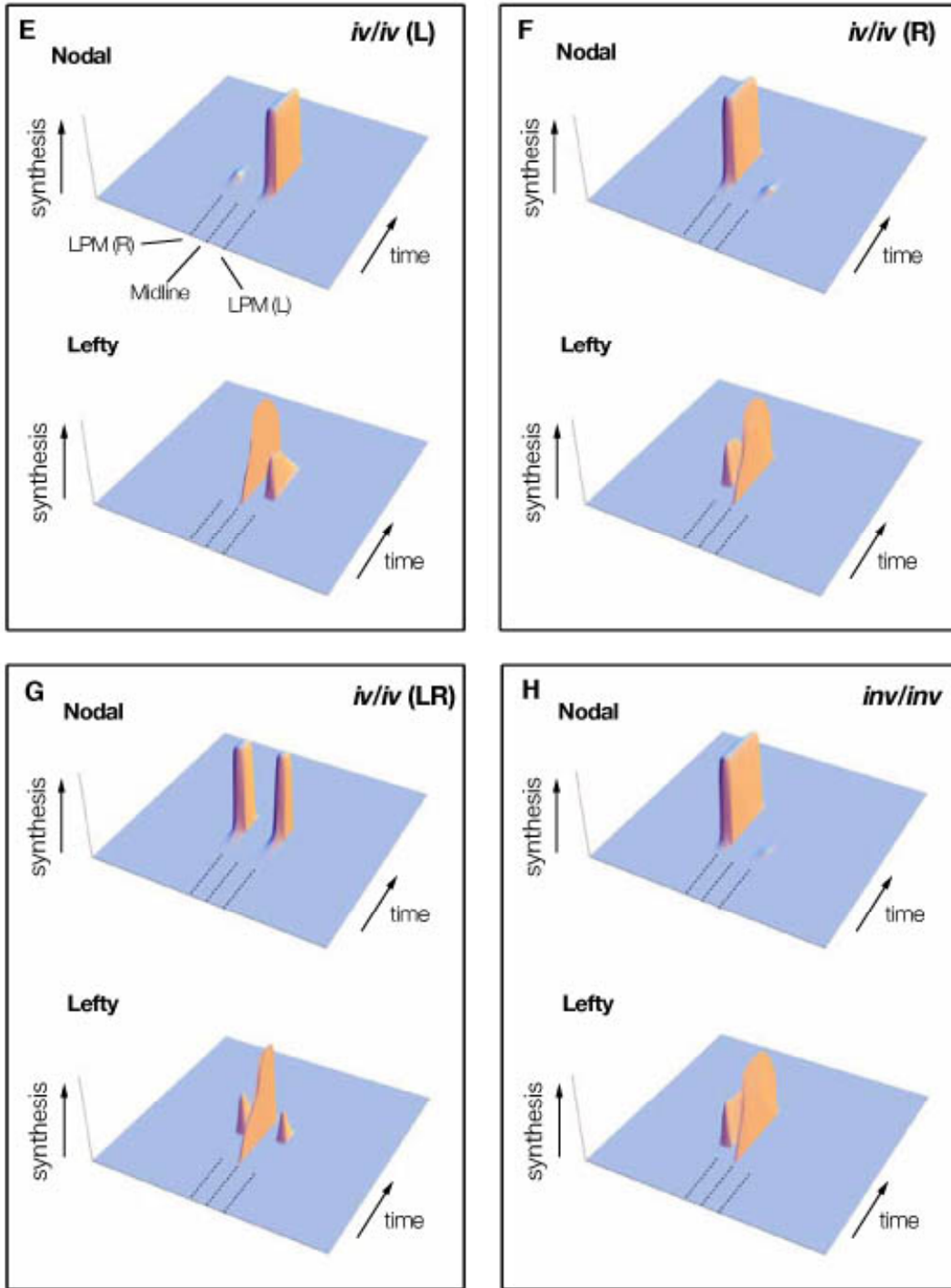


Figure S3-2

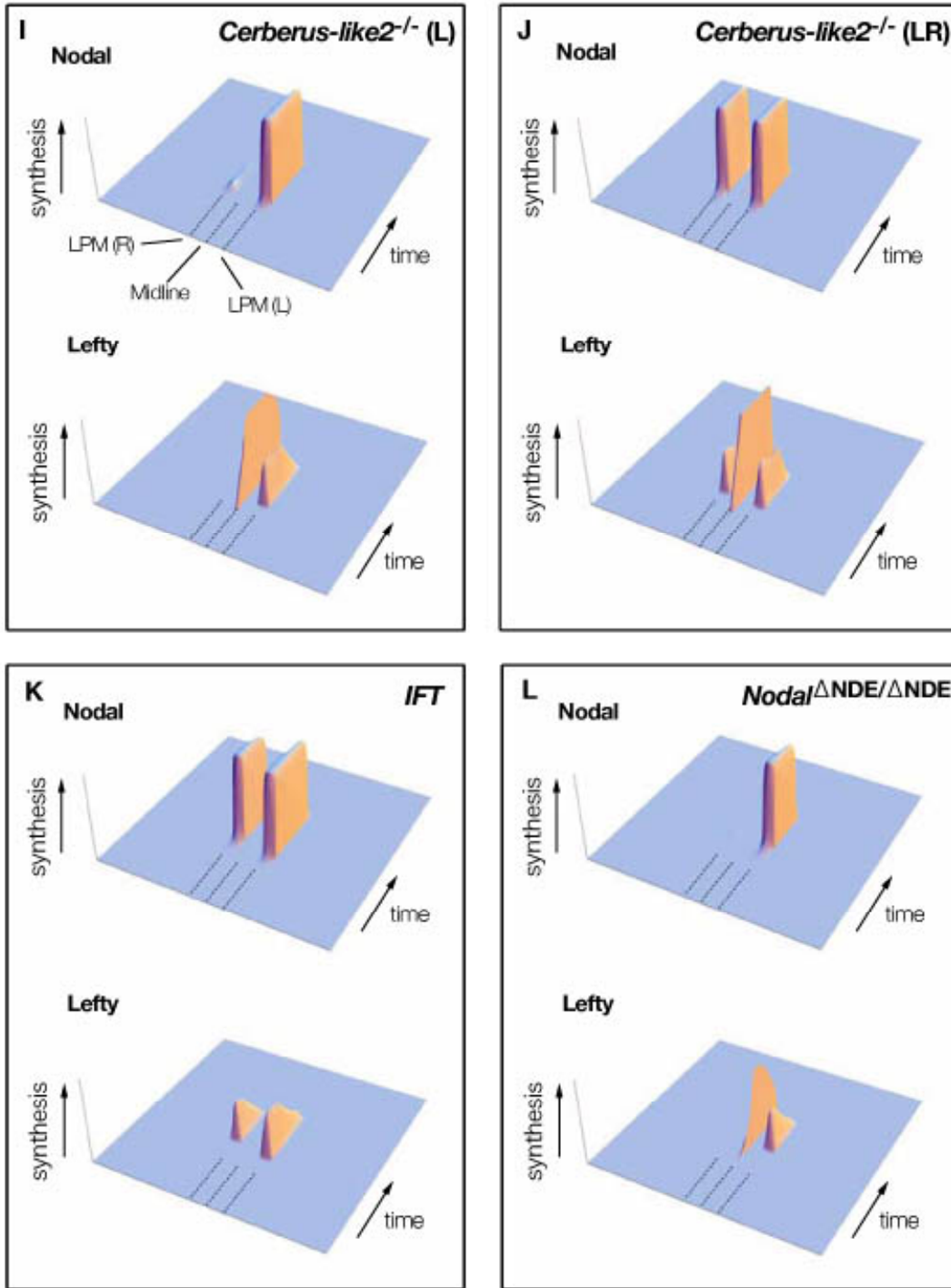


Figure S3-3

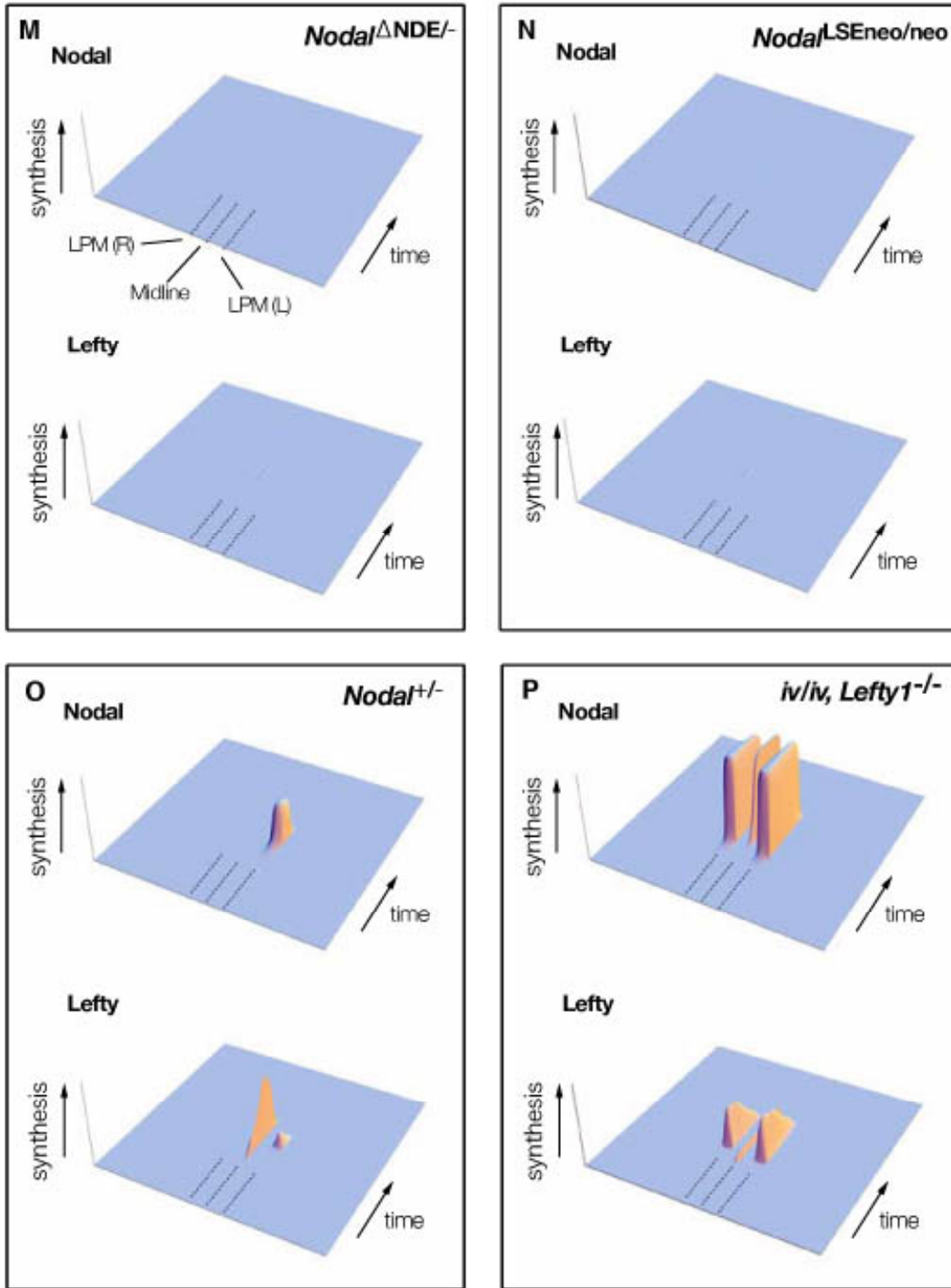


Figure S3-4

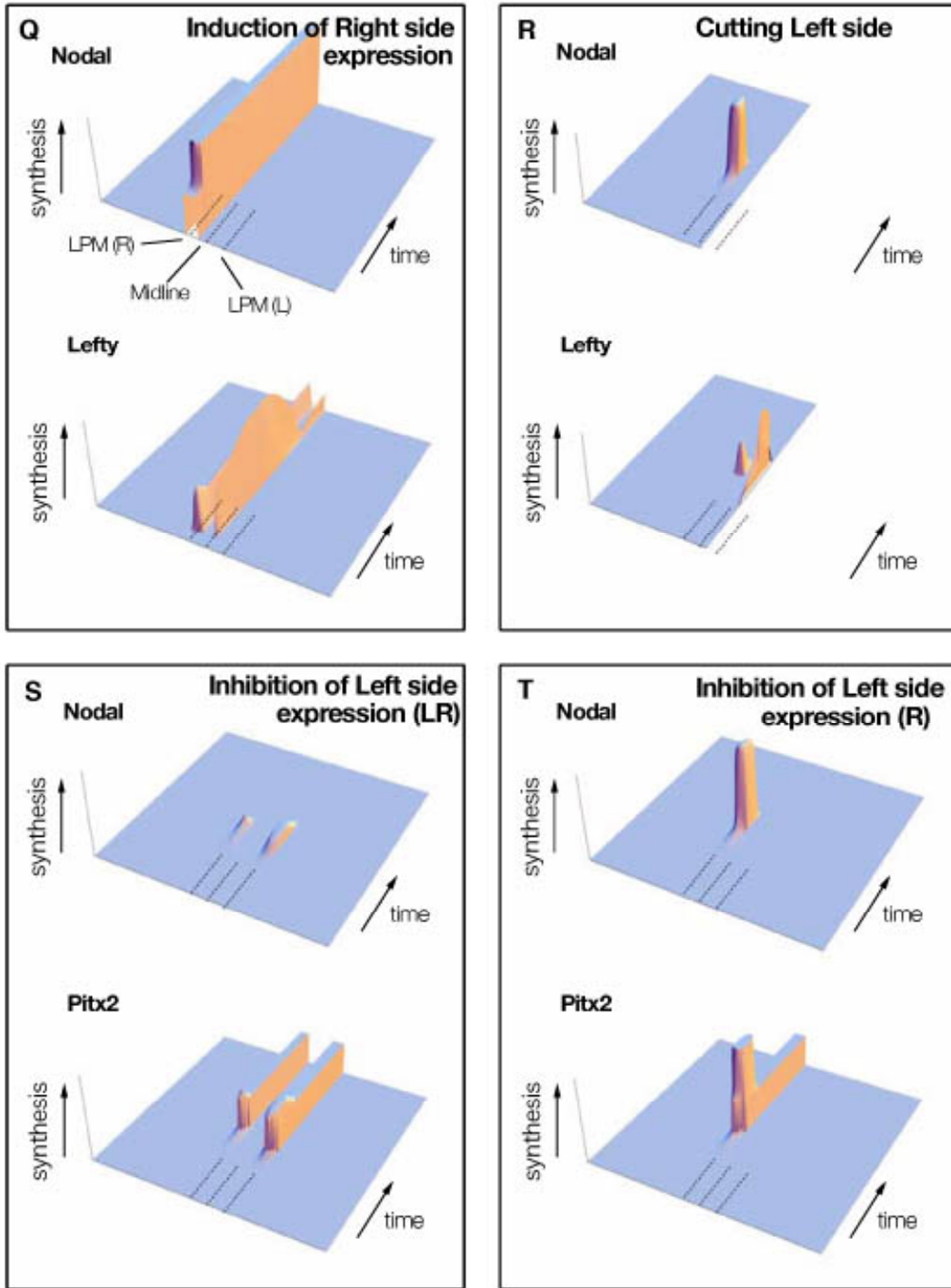


Figure S3-5

Supplemental Figure Legends

Figure S1. Timing of *Nodal*, *Lefty1*, and *Lefty2* Expression in Wild-Type Mouse Embryos.

(A–F) Simultaneous detection of *Nodal* and *Lefty1* mRNAs at the three-somite (A, B), four-somite (C, D), or five-somite (E, F) stages. *Nodal* is expressed in the node and left LPM whereas *Lefty1* is expressed in the floor plate (at the midline). Anterior views are shown (A), (C), and (E), a distal view in (B), and posterior views in (D) and (F). Dotted line in (B) indicates the level of the node. Arrowheads in (C) and (E) indicate edges of *Nodal* expression.

(G–L) Expression of *Nodal* (red) and *Lefty2* (blue) was examined by two-color in situ hybridization in embryos at the three-somite (G), four-somite (I), five-somite (H, J, K), or six-somite (L) stages. Anterior views are shown in all panels. Red and blue arrowheads indicate edges of *Nodal* and *Lefty2* expression respectively.

Thus, *Nodal* expression begins in the node at embryonic day (E) 7.5. *Lefty1* expression, most likely induced by *Nodal*, begins at the midline near the node at the two-somite stage and extends anteriorly. *Nodal* expression in LPM begins in the region adjacent to the node and expands along the anteroposterior axis. Expression of *Lefty2* then follows that of *Nodal*.

Figure S2. Qualitative Behavior of a Simple Mathematical Model

Several different patterns can arise from a simple mathematical model. Four of such patterns are shown here while the remaining one is shown in Figure 2B.

(A) One of the “Signal-dependent amplification” patterns. The dynamics will converge to the intersection point after transient amplification when N_i is large enough (blue arrows) or it will converge to zero without amplification when N_i is small (red arrow). (B, C) “Bi-stable” patterns. The dynamics will converge to two stable equilibria.

(D) “Stable at the origin” pattern. The dynamics converge to the single stable equilibrium at the origin.

(E) Qualitative behavior of *Nodal* and *Lefty* in right LPM.

(F) Qualitative behavior of *Nodal* and *Lefty* in left LPM. (E) and (F) are shown by a magnified scale in contrast to (A)-(D).

Figure S3. Simulation of L-R Asymmetric Expression of *Nodal* and *Lefty* in Embryos of Various Mutant Mice

Values of the model parameters used for the various mutants are provided in Supplementary Table S1; those altered in some of the mutants are described below:

Lefty1^{+/-}

S_{L0} are reduced to 55% of the corresponding wild type values. L-R pattern is normal (Meno et al., 1998).

Lefty1^{-/-}

S_{L0} are reduced to 10% of the corresponding wild type values. A normal L-R pattern is established as a result of compensation by *Lefty2* (Meno et al., 1998).

Lefty2^{+/ Δ ASE}

S_{L1} and S_{L2} are reduced to one-half of the corresponding wild-type values. L-R pattern is normal (Meno et al., 2001).

Lefty2 ^{Δ ASE/ Δ ASE}

S_{L1} and $S_{L2} = 0$. *Nodal* expression in the left LPM and *Lefty1* expression in the midline persist for a longer period, as has been observed in *Lefty2* ^{Δ ASE/ Δ ASE} embryos (Meno et al., 2001).

Nodal^{+/-}

S_{N0}, S_{N1} and S_{N2} are set to one-half of the corresponding values for the wild type. f_{i0}, f_{i1} , and f_{i2} are reduced to about 80% of those for the wild type, given that the level of *Nodal* expression in the node of *Nodal*^{+/-} embryos as determined by in situ hybridization is only slightly reduced (data not shown). Asymmetric *Nodal* expression in LPM occurs normally (Collignon et al., 1996).

Nodal ^{Δ NDE/ Δ NDE}

In the absence of the node-specific enhancer (NDE) of *Nodal*, *Nodal* expression in the node is down-regulated (Brennan et al., 2002). f_{i0}, f_{i1} , and f_{i2} are reduced to about 60% of those for the wild type ($Nodal^{+/+} > Nodal^{+/-} > Nodal^{\Delta NDE/\Delta NDE} > Nodal^{LSE^{neo/neo}} > Nodal^{\Delta NDE/-} > Nodal^{-/-} = 0$). However, asymmetric *Nodal* expression in LPM takes place normally, as previously observed with the *Nodal* ^{Δ NDE/ Δ NDE} embryo (Brennan et al., 2002).

Nodal ^{Δ NDE/-}

In contrast to the *Nodal* ^{Δ NDE/ Δ NDE} mutant, which manifests asymmetric *Nodal* expression in LPM, the *Nodal* ^{Δ NDE/-} mutant lacks *Nodal* expression in LPM (Brennan et al., 2002).

f_{i0} , f_{i1} , and f_{i2} are reduced to one-half of those for the $Nodal^{\Delta NDE/\Delta NDE}$ mutant.

$Nodal\ LSE^{neo/neo}$

Replacement of the left side-specific enhancer (LSE) of *Nodal* with the neomycin phosphotransferase gene (*neo*) results in a marked reduction in *Nodal* expression in the node (Saijoh et al., 2003). Therefore, f_{i0} , f_{i1} , and f_{i2} are reduced to about 30% of those for the wild type. As we observed with the $Nodal\ LSE^{neo/neo}$ embryo, *Nodal* expression in LPM was absent in the simulation.

$Cer2^{-/-}$

$Cer2^{-/-}$ embryos exhibit bilateral (60%) or left-sided (30%) *Nodal* expression in LPM (Marques et al., 2004). In the absence of the Nodal inhibitor (Cerberus-like 2) at the node, the level of the Nodal signal at the node would be expected to increase. Therefore, f_{i0} , f_{i1} , and f_{i2} are set to higher values (f_{i2} increases more than f_{i1} does because the level of *Cer2* expression in the wild-type embryo is higher on the right side); smaller or larger increases in f_{i2} result in left-sided or bilateral expression of *Nodal* in LPM, respectively.

iv/iv

In the absence of nodal flow, there would be expected to be no bias between f_{i1} and f_{i2} , so that these parameters would fluctuate. Depending on the size of the difference that is spontaneously generated, *Nodal* expression in LPM is either right sided, left sided, or bilateral (Lowe et al., 1996).

IFT mutants

Several mutant mice have been described that lack a component of intraflagellar transport (IFT), such as Polaris (Murcia et al., 2000), KIF3a (Takeda et al., 1999), or IFT172 (Huangfu et al., 2003). Because these mutants lack nodal flow, f_{i1} and f_{i2} are set as in *iv/iv* embryos. In addition, IFT mutants have midline defects characterized by a lack of *Lefty1* and *Lefty2* expression at the midline. Therefore, S_{N0} and S_{L0} are 0. *Nodal* and *Lefty2* expression is bilateral in LPM and persists for a longer period.

inv/inv

f_{i1} is set to less than f_{i2} . The *Nodal* expression pattern is reversed (Lowe et al., 1996).

Inhibition of the left side

An *EGFP-Lefty2* expression vector was introduced into the left LPM as shown in Figure 2. S_N , S_L and S_P are reduced to 0 (complete inhibition) or 5 (partial inhibition).

Removal of the left LPM

Embryonic explants with left LPM removed were cultured. The simulation was

performed in the region that lacks “left LPM” and “left PAM”.

Activation on the right side

A *Nodal* expression vector was introduced into the right LPM as in Figure 1. The +20 term was therefore added to the Nodal equation for the right LPM. *Nodal* expression in LPM is right sided.

	WT	<i>Lefty1</i> ^{+/-}	<i>Lefty1</i> ^{-/-}	<i>Lefty2</i> ^{+/ΔASE}	<i>Lefty2</i> ^{ΔASE/ΔASE}	<i>iv/iv</i> (L)
<i>D_N</i>	20	20	20	20	20	20
<i>D_W</i>	40	40	40	40	40	40
<i>S_{N1}, S_{N2}</i>	40	40	40	40	40	40
<i>S_{N0}</i>	40	40	40	40	40	40
<i>S_{L1}, S_{L2}</i>	40	40	40	20	0	40
<i>S_{L0}</i>	40	22	4	40	40	40
<i>S_{P1}, S_{P2}</i>	40	40	40	40	40	40
<i>S_{P0}</i>	40	40	40	40	40	40
<i>S_q</i>	15	15	15	15	15	15
<i>T_{N1}, T_{N2}</i>	13	13	13	13	13	13
<i>T_{N0}</i>	13	13	13	13	13	13
<i>T_{L1}, T_{L2}</i>	18	18	18	18	18	18
<i>T_{L0}</i>	5	5	5	5	5	5
<i>T_{P1}, T_{P2}</i>	13	13	13	13	13	13
<i>T_{P0}</i>	13	13	13	13	13	13
<i>T_q</i>	2.3	2.3	2.3	2.3	2.3	2.3
$\lambda_{N1}, \lambda_{N2}$	1	1	1	1	1	1
λ_{N0}	1	1	1	1	1	1
$\lambda_{L1}, \lambda_{L2}$	1	1	1	1	1	1
λ_{L0}	4	4	4	4	4	4
$\lambda_{P1}, \lambda_{P2}$	1	1	1	1	1	1
λ_{P0}	1	1	1	1	1	1
λ_q	30	30	30	30	30	30
<i>g_{N1}, g_{N2}</i>	1	1	1	1	1	1
<i>g_{N0}</i>	1	1	1	1	1	1
<i>g_{L1}, g_{L2}</i>	2.5	2.5	2.5	2.5	2.5	2.5
<i>g_{L0}</i>	1.5	1.5	1.5	1.5	1.5	1.5
<i>d_N</i>	0.5	0.5	0.5	0.5	0.5	0.5
<i>d_L</i>	0.1	0.1	0.1	0.1	0.1	0.1
<i>d_P</i>	0.5	0.5	0.5	0.5	0.5	0.5
<i>f₁₀</i>	0.3	0.3	0.3	0.3	0.3	0.3
<i>f₁₁</i>	1.5	1.5	1.5	1.5	1.5	1.2
<i>f₁₂</i>	1	1	1	1	1	1.05

Table S1

	iv/iv (R)	iv/iv (LR)	inv/inv	$Cerberus-like2^{+}(L)$	$Cerberus-like2^{+}(LR)$	IFT
D_N	20	20	20	20	20	20
D_W	40	40	40	40	40	40
S_{N1}, S_{N2}	40	40	40	40	40	40
S_{N0}	40	40	40	40	40	0
S_{L1}, S_{L2}	40	40	40	40	40	40
S_{L0}	40	40	40	40	40	0
S_{P1}, S_{P2}	40	40	40	40	40	40
S_{P0}	40	40	40	40	40	0
S_q	15	15	15	15	15	15
T_{N1}, T_{N2}	13	13	13	13	13	13
T_{N0}	13	13	13	13	13	13
T_{L1}, T_{L2}	18	18	18	18	18	18
T_{L0}	5	5	5	5	5	5
T_{P1}, T_{P2}	13	13	13	13	13	13
T_{P0}	13	13	13	13	13	13
T_q	2.3	2.3	2.3	2.3	2.3	2.3
$\lambda_{N1}, \lambda_{N2}$	1	1	1	1	1	1
λ_{N0}	1	1	1	1	1	1
$\lambda_{L1}, \lambda_{L2}$	1	1	1	1	1	1
λ_{L0}	4	4	4	4	4	4
$\lambda_{P1}, \lambda_{P2}$	1	1	1	1	1	1
λ_{P0}	1	1	1	1	1	1
λ_q	30	30	30	30	30	30
g_{N1}, g_{N2}	1	1	1	1	1	1
g_{N0}	1	1	1	1	1	1
g_{L1}, g_{L2}	2.5	2.5	2.5	2.5	2.5	2.5
g_{L0}	1.5	1.5	1.5	1.5	1.5	1.5
d_N	0.5	0.5	0.5	0.5	0.5	0.5
d_L	0.1	0.1	0.1	0.1	0.1	0.1
d_P	0.5	0.5	0.5	0.5	0.5	0.5
f_{i0}	0.3	0.3	0.3	0.6	0.9	0.3
f_{i1}	1.05	1.03	1.1	1.7	1.9	1.2
f_{i2}	1.2	0.98	1.4	1.4	1.8	0.93

Table S2

	$Nodal^{+/}$	$Nodal^{\Delta NDE/\Delta NDE}$	$Nodal^{LSE\ neo/neo}$	$Nodal^{\Delta NDE/-}$	Inhibition of left(R)	Inhibition of left(LR)
D_N	20	20	20	20	20	20
D_W	40	40	40	40	40	40
S_{N1}, S_{N2}	20	40	40	20	0(only left)	5(only left)
S_{N0}	20	40	40	20	40	40
S_{L1}, S_{L2}	40	40	40	40	0(only left)	5(only left)
S_{L0}	40	40	40	40	40	40
S_{P1}, S_{P2}	40	40	40	40	40	40
S_{P0}	40	40	40	40	40	40
S_q	15	15	15	15	15	15
T_{N1}, T_{N2}	13	13	13	13	13	13
T_{N0}	13	13	13	13	13	13
T_{L1}, T_{L2}	18	18	18	18	18	18
T_{L0}	5	5	5	5	5	5
T_{P1}, T_{P2}	13	13	13	13	13	13
T_{P0}	13	13	13	13	13	13
T_q	2.3	2.3	2.3	2.3	2.3	2.3
$\lambda_{N1}, \lambda_{N2}$	1	1	1	1	1	1
λ_{N0}	1	1	1	1	1	1
$\lambda_{L1}, \lambda_{L2}$	1	1	1	1	1	1
λ_{L0}	4	4	4	4	4	4
$\lambda_{P1}, \lambda_{P2}$	1	1	1	1	1	1
λ_{P0}	1	1	1	1	1	1
λ_q	30	30	30	30	30	30
g_{N1}, g_{N2}	1	1	1	1	1	1
g_{N0}	1	1	1	1	1	1
g_{L1}, g_{L2}	2.5	2.5	2.5	2.5	2.5	2.5
g_{L0}	1.5	1.5	1.5	1.5	1.5	1.5
d_N	0.5	0.5	0.5	0.5	0.5	0.5
d_L	0.1	0.1	0.1	0.1	0.1	0.1
d_P	0.5	0.5	0.5	0.5	0.5	0.5
f_{i0}	0.24	0.18	0.09	0.09	0.3	0.3
f_{i1}	1.2	0.9	0.45	0.45	1.5	1.5
f_{i2}	0.8	0.6	0.3	0.3	1	1

Table S3

	$iv/iv, LeftyI^{+}$	Activation of right
D_N	20	20
D_W	40	40
S_{N1}, S_{N2}	40	40
S_{N0}	40	40
S_{L1}, S_{L2}	40	40
S_{L0}	4	40
S_{P1}, S_{P2}	40	40
S_{P0}	40	40
S_q	15	15
T_{N1}, T_{N2}	13	13
T_{N0}	13	13
T_{L1}, T_{L2}	18	18
T_{L0}	5	5
T_{P1}, T_{P2}	13	13
T_{P0}	13	13
T_q	2.3	2.3
$\lambda_{N1}, \lambda_{N2}$	1	1
λ_{N0}	1	1
$\lambda_{L1}, \lambda_{L2}$	1	1
λ_{L0}	4	4
$\lambda_{P1}, \lambda_{P2}$	1	1
λ_{P0}	1	1
λ_q	30	30
g_{N1}, g_{N2}	1	1
g_{N0}	1	1
g_{L1}, g_{L2}	2.5	2.5
g_{L0}	1.5	1.5
d_N	0.5	0.5
d_L	0.1	0.1
d_P	0.5	0.5
f_{i0}	0.3	0.3
f_{i1}	1.2	1.5
f_{i2}	1.05	1

Table S4

Supplemental Table Legend

Table S1. Parameters for the SELI system used to simulate L-R asymmetric gene expression in embryos of wild-type and various mutant mice. Parameters set to values different from those in the wild type are shaded. For the “activation of right” condition, we added the term +20 to the Nodal equation for the right side.